Journal of Engineering Mathematics (2006) 54: 273–298
DOI 10.1007/s10665-005-9025-y

Interactions of inert confiners with explosives

G.J. SHARPE[1,2] and J.B. BDZIL[1]
[1]*Los Alamos National Laboratory, Los Alamos, New Mexico 87545, USA (E-mail: mengjs@leeds.ac.uk; jbb@lanl.gov);*
[2]*Current address: School of Mechanical Engineering, University of Leeds, Leeds LS2 9JT, UK*

Received 26 April 2005; accepted in revised form 10 November 2005 / Published online: 24 January 2006

Abstract. The deformation of an inert confiner by a steady detonation wave in an adjacent explosive is investigated for cases where the confiner is sufficiently strong (or the explosive sufficiently weak) such that the overall change in the sound speed of the inert is small. A coupling condition which relates the pressure to the deflection angle along the explosive-inert interface is determined. This includes its dependence on the thickness of the inert, for cases where the initial sound speed of the inert is less than or greater than the detonation speed in the explosive (supersonic and subsonic inert flows, respectively). The deformation of the inert is then solved by prescribing the pressure along the interface. In the supersonic case, the detonation drives a shock into the inert, subsequent to which the flow in the inert consists of alternating regions of compression and tension. In this case reverberations or 'ringing' occurs along both the deflected interface and outer edge of the inert. For the subsonic case, the flow in the interior of the inert is smooth and shockless. The detonation in the explosive initially deflects the smooth interface towards the explosive. For sufficiently thick inerts in such cases, it appears that the deflection of the confiner would either drive the detonation speed in the explosive up to the sound speed of the inert or drive a precursor wave ahead of the detonation in the explosive. Transonic cases, where the inert sound speed is close to the detonation speed, are also considered. It is shown that the confinement affect of the inert on the detonation is enhanced as sonic conditions are approached from either side.

Key words: detonation, explosives, shock waves, transonic

1. Introduction

In many applications of condensed-phase (solid or liquid) explosives, the explosive is surrounded by or adjacent to an inert medium, which, if sufficiently strong, has a 'confinement effect' on the propagation of a detonation wave in the explosive. Of interest for applications is not only how the confinement affects the dynamics, shape and speed of the detonation wave, but also what the detonated explosive does to the surrounding inert. The lateral confinement provided by an adjacent inert acts to support the high pressure generated in the detonation reaction zone, thereby helping to sustain detonation in even thin samples of explosive. Conversely, the high detonation pressures can be used to both accelerate confinement layers, such as in the copper-cylinder test, *e.g.* [1], or to fragment rock, as when explosive is detonated in a bore hole for mining.

The interaction between the detonation dynamics in the explosive and the deformation of the confining inert is highly coupled. A first step towards understanding the types of interactions that can occur involves performing a standard shock polar match at the point where the shock waves intersect the explosive-inert interface, *e.g.* [2]. Figure 1(a) shows a diagram of the flow near the shock-interface intersection point. This diagram is based on the assumption that the flow in the reaction zone is subsonic as measured in the reference frame of the shock-interface intersection point: steady and subsonic flow precludes the existence of any reflected

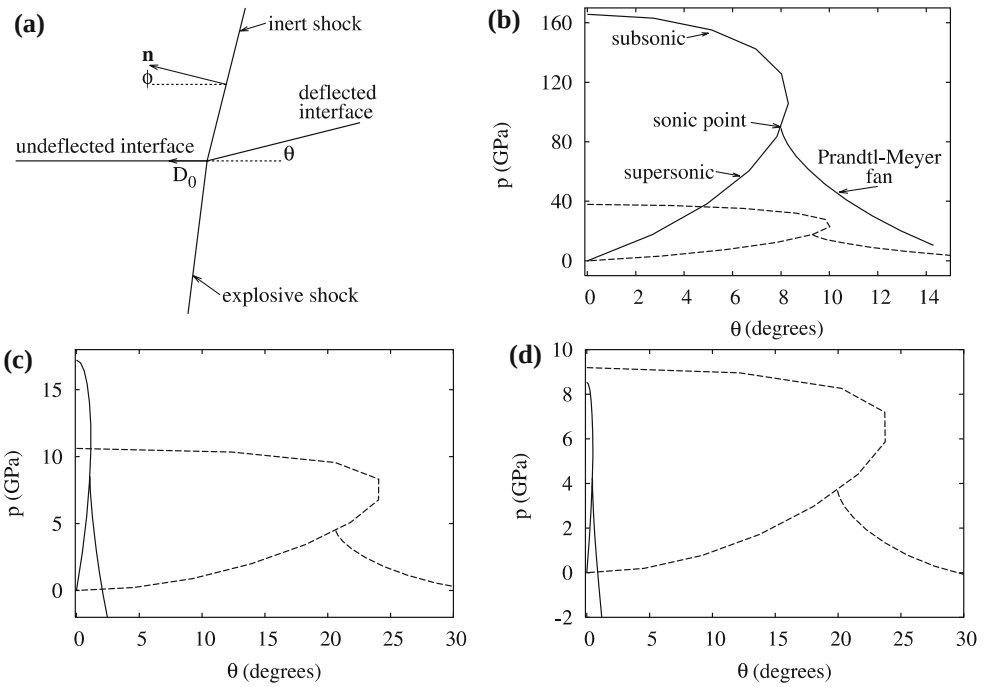

Figure 1. (a) Schematic of structure near intersection of shocks and explosive-inert interface, and shock polars (shock pressure against streamline-deflection angle) for (b) copper (solid lines) and unreacted PBX 9502 explosive (dashed lines) running at $D_0 = 7{\cdot}60$ km/s, (c) copper (solid lines) and ANFO (dashed lines) running at $D_0 = 4{\cdot}55$ km/s and (d) copper (solid lines) and ANFO (dashed lines) running at $D_0 = 4{\cdot}25$ km/s.

shock back into the explosive (since steady, subsonic flows admit only smooth solutions, as they are governed by elliptic partial differential equations).

In either material, given the speed at which the shock propagates along the undeflected interface, D_0, (which is the detonation speed for a steady detonation propagating along a cylinder or slab of confined explosive) and the angle which the shock normal makes with the undisturbed interface, ϕ, the standard shock jump conditions give the shock pressure and post-shock interface (streamline) deflection angle, θ. Increasing the shock normal angle, ϕ, results in an interface deflection angle-shock pressure curve, *e.g.* as shown in Figure 1(b), where the upper-branch curve corresponds to a subsonic shocked state and the lower branch corresponds to a supersonic shocked state. There is a maximum streamline deflection that can occur via an oblique shock. This value is referred to a the Crocco point [3]. For sufficiently weak confinement or no confinement the streamline deflection in the explosive can exceed what is possible from a simple oblique shock state. Under these conditions, a reflected Prandtl-Meyer fan centred at the sonic flow state of the shock allows the streamline angle to increase further and pressure to drop (all the way to zero for a completely unconfined explosive); *e.g.* [4]. Since the pressures and streamline-deflection angles in the explosive and in the inert confiner must match at the interface, the points where the explosive and inert shock polars cross give the possible solutions (shock normal angles, shock pressures and interface deflection angles) for a given explosive-inert pair and detonation speed, D_0.

Several types of possible matches are shown in Figure 1. Figure 1(b) shows theoretical calculations of shock polars for the high-density explosive PBX 9502 confined by copper. In this case, the match point is such that the post-shock flow in the PBX 9502 is subsonic at the interface, while it occurs on the low pressure branch of the copper shock polar, so that the

flow is supersonic in the confiner. This type of match is the typical case for high explosives confined by metals.

However, for weak explosives as typically used in mining applications and by terrorists, such as ammonium nitrate fuel-oil (ANFO), one finds different types of matches. Two feature changes are noteworthy: (i) the pressures and detonation speed are reduced substantially; (ii) owing to the porous nature of such explosives, the streamline turning angles can achieve greatly increased values. For example, Figure 1(c) shows theoretical shock polars for copper confining a porous ANFO for a detonation speed of 4·55 km/s. In this case the match point of interest occurs on the upper branches of both explosive and inert, so that the post-shock flow is subsonic in both materials. Figure 1(d) shows a similar plot, but when the detonation speed in the ANFO is 4·25 km/s. It should be noted that the detonation speed depends on both the diameter of the explosive charge and on the thickness of the confining inert; a decrease in explosive charge diameter leads to a decrease in detonation speed. For $D_0 = 4{\cdot}25$ km/s there is no match point for the shock polars, apart from a nonphysical very small pressure and deflection angle. This is because for lower detonations speeds, the sound speed of the pressurized copper becomes greater than the detonation speed. There is, of course, still a solution for such problems, but it consists of a totally shock-free, subsonic flow in the confiner. Such a situation rarely exists for high explosives. The one notable exception is when beryllium serves as a confiner for the high explosive PBX 9502.

Although the shock polar matches give an indication of the different types of interactions that can occur for a given explosive-confiner pair, it is important to note that it is a point match, *i.e.*, it only tells one the conditions at the point of intersection of the shocks and the interface. The shock-polar match gives no information about the flow in the interior of the explosive or the inert. For the propagation of detonation in the explosive, there exists a set of rigorous asymptotic theories called detonation shock dynamics (DSD), based on the limit of small shock curvature. See [5] for a review. DSD determines the speed of the detonation and the shape of the shock in the explosive in addition to determining the structure of the detonation reaction zone.

However, Bdzil [4] found that, for confined explosives, there exists a boundary layer in the explosive of size $O(\theta)$ (where $\theta \ll 1$) adjacent to the interface where the DSD approximations break down. Bdzil [4] did not obtain the detailed solution in this region, but instead determined a coupling condition between the pressure along the interface and the interface deflection. This was done for the case of an infinitely thick inert and a supersonic inert polar match point. Bdzil [4] then used this condition to determine the shock-normal-angle boundary condition to be applied at the edge of the DSD region of the explosive, which gives a modified edge shock angle to that predicted by the shock polar match. In order to solve the complete problem, *i.e.*, the flow in both the DSD region and edge boundary layer of the explosive, together with the solution in the inert, one requires a coupling condition between the explosive and the inert, *i.e.*, a relationship between the pressure and the deflection angle along the interface.

The purpose of this paper is to (i) determine the interfacial coupling conditions between the explosive and inert, including how this condition depends on the thickness of the inert; (ii) classify the different types of explosive-inert interactions that may occur; (iii) determine the types of inert deformations that detonations can induce. In order to achieve these results, we consider the asymptotic limit where the inert confiner is sufficiently strong such that the disturbances to the inert induced by the detonation in the explosive are weak.

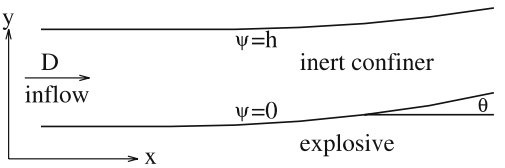

Figure 2. Explosive-shock fixed Cartesian co-ordinates for the deformation in the inert confiner, $\psi = 0$ is the explosive-inert interface and $\psi = h$ is the outer boundary. (Shock waves are also possible in the inert – not shown in schematic).

2. The model and governing equations

Here we consider a slab of explosive which is adjacent to a slab of a confining inert of thickness h. The geometry of the problem is shown in Figure 2. We consider the steady-state problem, such that a detonation propagates through the explosive at constant speed D (which will in general depend both on the thickness of the explosive slab and the nature and thickness of the confining inert). The detonation is assumed to propagate right to left in the laboratory frame. We work in the detonation rest frame, such that the upstream flow is oncoming with speed D, and the point where the explosive shock intersects the explosive-inert interface is at $x = 0$.

Since the typical detonation-induced pressures are very high, we make the assumption that the deformation of the inert can be described by the Euler equations [6]. However, here we use the x-coordinate and the stream function, ψ, as the independent variables so that y is then one of the solution state-dependent variables [7, pp. 182–184]. The dimensionless governing equations are then

$$\frac{\partial y}{\partial x} = \frac{v}{u}, \quad \frac{\partial y}{\partial \psi} = \frac{1}{\rho u}, \quad \frac{\partial v}{\partial x} + \frac{\partial p}{\partial \psi} = 0, \tag{1}$$

$$c^2 = \left(\frac{\mathrm{d}p}{\mathrm{d}\rho}\right)_S = \left[\frac{p}{\rho^2} - \left(\frac{\partial e}{\partial \rho}\right)\right]\left(\frac{\partial e}{\partial p}\right)^{-1}, \tag{2}$$

[7, pp. 182–184] together with Bernoulli's equation:

$$e(p, \rho) + \frac{p}{\rho} + \frac{1}{2}(u^2 + v^2) = e(p_0, \rho_0) + \frac{1}{2}, \tag{3}$$

where u and v are the material velocities in the x- and y-directions, respectively, as measured in the steady frame, ρ is the density, p is the pressure, c is the sound speed and $e(p, \rho)$ is the internal energy given by an equation of state for the inert (for example, Bdzil [4] considered a simple Tait equation of state, $e(p, \rho) = (p + an)/((n-1)\rho)$, with a and n constants). The zero subscript denotes values in the initial, quiescent state of the inert and the S subscript denotes evaluation at constant entropy. We have used the approximation that the upstream pressure is negligible, $p_0 \approx 0$. The streamline deflection angle at any point, θ, *i.e.*, the angle the streamline makes with the x-direction is given by

$$\tan\theta = \frac{v}{u}. \tag{4}$$

Here we have non-dimensionalized using the following scalings:

$$p = \frac{\tilde{p}}{\tilde{\rho}_0 \tilde{D}^2}, \quad u = \frac{\tilde{u}}{\tilde{D}}, \quad v = \frac{\tilde{v}}{\tilde{D}}, \quad \rho = \frac{\tilde{\rho}}{\tilde{\rho}_0}, \quad e = \frac{\tilde{e}}{\tilde{D}^2}, \quad c^2 = \frac{\tilde{c}^2}{\tilde{D}^2},$$

$$x = \frac{\tilde{x}}{\tilde{x}^*}, \quad y = \frac{\tilde{y}}{\tilde{x}^*}, \quad \psi = \frac{\tilde{\psi}}{\tilde{\rho}_0 \tilde{D} \tilde{x}^*}, \tag{5}$$

where a tilde denotes a dimensional quantity. Here the scaling for length, $\tilde{x}^*$, is chosen to be a characteristic length scale of the reaction zone in the explosive, measured at the interface. Hence the dimensionless initial thickness of the inert, h, is the ratio of the thickness of the inert slab to the interfacial reaction zone length scale.

Since the explosive and inert are in mechanical equilibrium, the boundary conditions to be applied along the explosive-inert interface, $\psi = 0$, are the assumed pressure profile of the detonation and following flow in the explosive along the interface, and the balancing of the components of material velocities normal to the interface across it.

The boundary conditions to be applied on the far side of the inert, $\psi = h$, depend on the confinement condition on the far side. Two simple possibilities are a free-boundary condition $p(\psi = h, x) = 0$ (the limit of no external material) or a rigid-wall condition $v(\psi = h, x) = 0$ (the limit of a very strong external material). For a very thin confining inert ($h \ll 1$), the explosive will not feel the inert, and hence in this case the free-boundary condition provides no confinement, while the rigid-wall condition provides perfect confinement. On the other hand, for a very thick inert confiner ($h \gg 1$), the far-side inert material boundary condition will have little effect on the explosive-confinement problem. Here we will mainly consider intermediate problems with $h = O(1)$ and consider both the free-boundary and rigid-wall problems.

Supplementary to Equations (1–3) we have the shock conditions. Suppose a shock exists in the inert along a locus $x = x_s(y)$, then the jump conditions give

$$\rho_s u_n = \cos\phi, \quad p_s + \rho_s u_n^2 = \cos^2\phi, \quad e(p_s, \rho_s) + \frac{p_s}{\rho_s} + \frac{1}{2}u_n^2 = e_0 + \frac{1}{2}\cos^2\phi, \tag{6}$$

$$u_t = \sin\phi, \tag{7}$$

where an 's' subscript denotes shock values, $\phi(y)$ is the angle the shock normal makes with the x-direction, and u_n and u_t are the components of the post-shock material velocity normal and tangent to the shock, respectively. Hence

$$\tan\phi = \frac{\mathrm{d}x_s}{\mathrm{d}y}, \quad v_s = \sin\phi\cos\phi - u_n\sin\phi, \quad u_s = \sin^2\phi + u_n\cos\phi, \tag{8}$$

$$\tan\theta_s = \frac{v_s}{u_s}, \tag{9}$$

where θ_s is the streamline-deflection angle at the shock.

We will consider the asymptotic limit that the typical dimensionless pressure $p = \tilde{p}/(\tilde{\rho}_0\tilde{D}^2)$ is small. Define the quantity $\delta = \tilde{p}_{Is}/(\tilde{\rho}_0\tilde{D}^2)$, where $\tilde{p}_{Is}$ is the explosive shock pressure at the interface, which is therefore the shock polar match value and hence the pressure in the inert at $(\psi, x) = (0, 0)$. For the examples in Figure 1, we find for the case of ANFO and copper ($\tilde{\rho}_0 \approx 9\,\mathrm{g/cm^3}$) with $\tilde{D} \approx 4{\cdot}5\,\mathrm{km/s}$, that $\delta \approx 0{\cdot}06$, while for PBX9502 and copper with $\tilde{D} = 7{\cdot}6\,\mathrm{km/s}$, then $\delta \approx 0{\cdot}07$. Hence this is a valid limit for a weak enough explosive or strong enough confinement.

We therefore expand the variables as

$$p = \delta p_1 + O(\delta^2), \quad \rho = 1 + \delta\rho_1 + O(\delta^2), \quad u = 1 + \delta u_1 + O(\delta^2), \quad v = \delta v_1 + O(\delta^2), \tag{10}$$

$$c^2 = c_0^2 + \delta c_1^2 + O(\delta^2), \quad y = y_0 + \delta y_1 + O(\delta^2), \quad \theta = \delta\theta_1 + O(\delta^2), \tag{11}$$

where, from Equation (2), $c_0^2 = -e_{\rho 0}/e_{p0}$, with

$$e_0 = e(0, 1), \quad e_{\rho 0} = \left(\frac{\partial e}{\partial \rho}\right)_{p=0,\rho=1}, \quad e_{p0} = \left(\frac{\partial e}{\partial p}\right)_{p=0,\rho=1}, \tag{12}$$

and we expand $e(p, \rho)$ as

$$e(p, \rho) = e_0 + \delta e_{p0} p_1 + \delta e_{\rho 0} \rho_1 + O(\delta^2). \tag{13}$$

Note our asymptotic assumption of small pressures in the inert is hence equivalent to small overall changes in the sound speed of the inert or small deflection angle of the interface.

Substituting in Equations (1) gives $y_0 = \psi$ at $O(1)$ and

$$\frac{\partial y_1}{\partial x} = v_1, \quad \frac{\partial y_1}{\partial \psi} = -(\rho_1 + u_1), \quad \frac{\partial v_1}{\partial x} + \frac{\partial p_1}{\partial \psi} = 0 \tag{14}$$

at $O(\delta)$, while Equation (3) gives

$$(e_{p0} + 1) p_1 + e_{\rho 0} \rho_1 + u_1 = 0 \tag{15}$$

at $O(\delta)$.

Expanding the shock jump conditions (6–9) gives

$$\rho_{1s} = \frac{1}{c_0^2} p_{1s}, \quad v_{1s} = p_{1s} \sqrt{\frac{1}{c_0^2} - 1}, \quad u_{1s} = -p_{1s}, \tag{16}$$

$$\tan \phi_0 = \sqrt{\frac{1}{c_0^2} - 1}, \quad \theta_{1s} = p_{1s} \sqrt{\frac{1}{c_0^2} - 1}. \tag{17}$$

Since, apart from shock waves, the flow is isentropic, Equation (2) gives, to leading order,

$$p_1 - c_0^2 \rho_1 = k, \tag{18}$$

where k is a constant (which may be different on different streamlines). If there are no shocks in the inert, then clearly $k = 0$ everywhere (since $p_1 = \rho_1 = 0$ in the initial inert state, *i.e.*, as $x \to -\infty$). If there is a shock, then $k = p_{1s} - c_0^2 \rho_{1s}$, where p_{1s} and ρ_{1s} are the values at the point where the streamline in question intersects the shock locus. However, in this case the first jump condition in (16) shows that again $k = 0$. Thus $\rho_1 = p_1 / c_0^2$ everywhere in the inert in either case.

Equation (15) then gives

$$u_1 = -p_1, \tag{19}$$

so that Equations (14) can be rewritten as

$$\frac{\partial y_1}{\partial x} = v_1, \quad p_1 = \left(1 - \frac{1}{c_0^2}\right)^{-1} \frac{\partial y_1}{\partial \psi}, \quad \frac{\partial v_1}{\partial x} + \frac{\partial p_1}{\partial \psi} = 0, \quad \theta_1 = v_1, \tag{20}$$

giving the following coupled set of equations for p_1 and v_1 (or θ_1):

$$\frac{\partial v_1}{\partial x} + \frac{\partial p_1}{\partial \psi} = 0, \quad \frac{\partial v_1}{\partial \psi} - \beta \frac{\partial p_1}{\partial x} = 0, \tag{21}$$

or alternatively a single equation for y_1:

$$\frac{\partial^2 y_1}{\partial \psi^2} + \beta \frac{\partial^2 y_1}{\partial x^2} = 0, \tag{22}$$

where

$$\beta = \left(1 - \frac{1}{c_0^2}\right). \tag{23}$$

Note that for supersonic flow in the inert ($1 > c_0^2$) $\beta < 0$, and hence Equation (22) is the (hyperbolic) wave equation with wavespeed $C = \sqrt{-\beta}$, while for subsonic flow ($1 < c_0^2$) $\beta > 0$ and Equation (22) is essentially the (elliptic) Laplace equation. Note also that for the expansions that lead to Equation (22) to be valid, we require $\beta = O(1)$. In Section 5 we determine the appropriate scalings for cases where $\beta = O(\delta)$, which leads to nonlinear transonic flows. In the following, we consider the supersonic and subsonic cases in turn, and for each we determine relationships between the pressure profile along the explosive-inert interface and the induced velocity (or deflection angle) of the interface.

3. Supersonic inert flow

For supersonic inert flows, the typical case for high explosives confined by metals, the shock in the explosive will drive a shock into the inert. From the shock jump conditions of Equation (16), to leading order the shock lies along the straight line locus $x_s = \psi\sqrt{1/c_0^2 - 1}$. Bdzil [4] previously considered the supersonic case, but for an infinitely thick inert.

The solution of the wave Equation (22) is of the form

$$y_1 = f(\xi) + g(\eta), \tag{24}$$

where

$$\xi = x + C\psi, \quad \eta = x - C\psi \tag{25}$$

are the characteristic co-ordinates. Equations (20) then give

$$p_1 = \frac{1}{C}[g'(\eta) - f'(\xi)], \quad v_1 = f'(\xi) + g'(\eta). \tag{26}$$

Hence the Riemann Invariants are

$$Cp_1 + v_1 = \text{constant} \quad \text{on} \quad \text{lines} \quad \eta = \text{constant} \tag{27}$$

and

$$Cp_1 - v_1 = \text{constant} \quad \text{on} \quad \text{lines} \quad \xi = \text{constant}. \tag{28}$$

In this case the problem is solved straightforwardly by the method of characteristics, which reveals that the solution for the finite thickness inert problem is split into a series of regions, as shown in Figure 3. Here we denote the pressure along the explosive-inert interface as $p_1(\psi = 0, x) = p_I(x)$, with $p_I = 0$ for $x < 0$ (undisturbed state ahead of the shock). We shall denote the value of v_1 along the explosive-inert interface by $v_I(x)$ and the pressure and velocity along the outer edge of the inert ($\psi = h$) by $p_h(x)$ and $v_h(x)$, respectively. For the free outer boundary problem $p_h(x) = 0$, while for the rigid outer boundary problem $v_h(x) = 0$.

The first region behind the shock, which is bounded to the right by the ξ-characteristic $x = -C\psi + 2Ch$, is not affected by the boundary condition at $\psi = h$ (note that for the infinite thickness inert case considered by Bdzil [4], the whole interior of the inert consists only of this first region). In this region all the ξ-characteristics originate on the leading-order shock locus $x = C\psi$. Using the shock conditions, Equation (16), on the ξ-characteristics we have

$$Cp_1 - v_1 = Cp_{1s} - v_{1s} = 0 \tag{29}$$

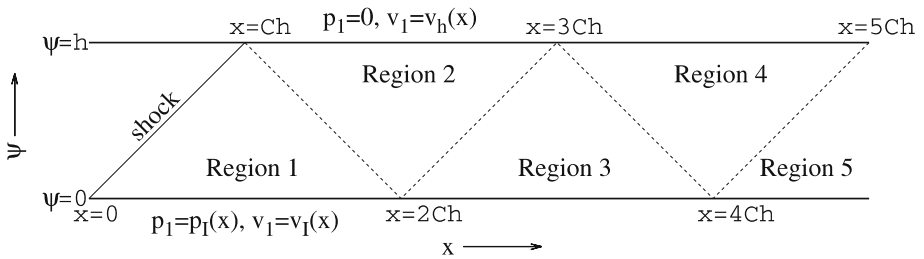

Figure 3. Solution regions for supersonic case (free outer boundary condition shown).

i.e., $v_1 = Cp_1$ everywhere in region 1. In particular $v_I(x) = Cp_I(x)$ on $\psi = 0$ for $0 \le x \le 2Ch$. Hence at a point (x, ψ) on any η-characteristics that pass through region 1, we have

$$Cp_1(x, \psi) + v_1(x, \psi) = 2Cp_I(x - C\psi), \tag{30}$$

where $x - C\psi$ is the point at which the η characteristics originated on $\psi = 0$. Thus within region 1, where $v_1 = Cp_1$,

$$p_1(x, \psi) = p_I(x - C\psi), \quad v_1(x, \psi) = Cp_I(x - C\psi). \tag{31}$$

Note that since the leading-order shock locus is itself the η-characteristic $x = C\psi$, we have

$$p_{1s} = p_I(0) = 1, \quad v_{1s} = Cp_I(0) = C \tag{32}$$

everywhere on the shock.

3.1. Free outer boundary

The solution in the subsequent regions depends on the choice of boundary condition on $\psi = h$. Here we consider first the free-outer-boundary case. Region 2 is bounded by the ξ-characteristic $x = -C\psi + 2Ch$ and the η-characteristic $x = C\psi + 2Ch$. The solution must be discontinuous across $x = -C\psi + 2Ch$, and hence also across subsequent region boundaries. Just to the left of $x = -C\psi + 2Ch$, the ξ-characteristics originate at the shock, where $p_1 = 1$, while just to the right of it the ξ-characteristics (which pass through region 2) originate from $\psi = h$, where $p_1 = 0$. Note that these discontinuities at the region boundaries represent to leading-order weak shocks or weak expansion fans in the full nonlinear problem.

Constructing the solution in region 2 by the method of characteristics, using the information from region 1, we have

$$p_1(x, \psi) = p_I(x - C\psi) - p_I(x + C\psi - 2Ch), \tag{33}$$

$$v_1(x, \psi) = Cp_I(x - C\psi) + Cp_I(x + C\psi - 2Ch). \tag{34}$$

Similarly, in the manner outlined above, we can proceed to obtain the solution in subsequent regions using information from previous ones. One finds that the general solution is

$$p_1(x, \psi) = \sum_{i=0}^{n-1} p_I(x - C\psi - 2iCh) - \sum_{i=1}^{n} p_I(x + C\psi - 2iCh), \tag{35}$$

$$v_1(x, \psi) = C\sum_{i=0}^{n-1} p_I(x - C\psi - 2iCh) + C\sum_{i=1}^{n} p_I(x + C\psi - 2iCh), \tag{36}$$

in solution region $2n$ ($n=2,3,4,\ldots$), and

$$p_1(x,\psi)=\sum_{i=0}^{n} p_I(x-C\psi-2iCh)-\sum_{i=1}^{n} p_I(x+C\psi-2iCh), \tag{37}$$

$$v_1(x,\psi)=C\sum_{i=0}^{n} p_I(x-C\psi-2iCh)+C\sum_{i=1}^{n} p_I(x+C\psi-2iCh) \tag{38}$$

in solution region $2n+1 (n=1,2,3,\ldots)$.

The y-velocity perturbations along the explosive-inert interface and outer edge of the inert are hence given by

$$v_I(x)=Cp_I(x)+2C\sum_{i=1}^{n} p_I(x-2iCh) \tag{39}$$

for $2nCh\le x\le(2n+2)Ch$, $n=1,2,3,\ldots$, and

$$v_h(x)=2C\sum_{i=1}^{n} p_I(x-(2i-1)Ch) \tag{40}$$

for $(2n-1)Ch\le x\le(2n+1)Ch$, $n=1,2,3,\ldots$. Equation (39) is the principal result of this section. It relates the pressure along the interface to the deflection angle of the interface and gives the interfacial coupling boundary condition with which one can determine how the flow in the explosive reaction zone is influenced by the confinement and vice versa. Since $v_I(x)\propto C$, then as $C\to 0$, *i.e.*, as the detonation speed approaches the sound speed of the inert, the interface deflection also tends to zero. Equation (39) therefore shows that the confinement effect of the inert is enhanced as sonic-flow conditions, $C=0$, are approached. However, it should be noted that, as $C\to 0$, nonlinear effects must be re-instated as the flow becomes of transonic type; see Section 5.

Denoting the y-position perturbation of the explosive-inert interface and the outer edge of the inert by $y_I(x)$ and $y_h(x)$, respectively, these quantities are given by

$$\frac{\mathrm{d}y_I}{\mathrm{d}x}=v_I(x),\quad \frac{\mathrm{d}y_h}{\mathrm{d}x}=v_h(x). \tag{41}$$

Equation (41) together with Equation (39) give a further relationship between the pressure along the explosive-inert interface and shape of the deflected interface.

Of course, the complete solution in the explosive and the inert is a coupled problem. However, in order to explore the types of deformations one may expect to occur in the inert, we can now determine the solution in the interior of the inert by prescribing the interfacial pressure, p_I. As an example, we consider the case where the interface pressure is prescribed by a shock jump followed by a two-step exponential decay of the form

$$p_I(x)=\begin{cases} H(1-x)\exp(-\alpha_1 x)+H(x-1)\exp(-\alpha_1-\alpha_2(x-1)), & x>0,\\ 0, & x\le 0.\end{cases} \tag{42}$$

This interface loading is designed to mock up the typical decaying pressure profile along streamlines in the explosive, *i.e.*, the detonation reaction zone followed by the pressure release wave in the detonation products. In summary, this interface loading begins with a shock discontinuity at $x=0$, followed by a first decay step, corresponding to the explosive reaction zone, which is followed by a the second decay step, corresponding to the detonation products release wave.

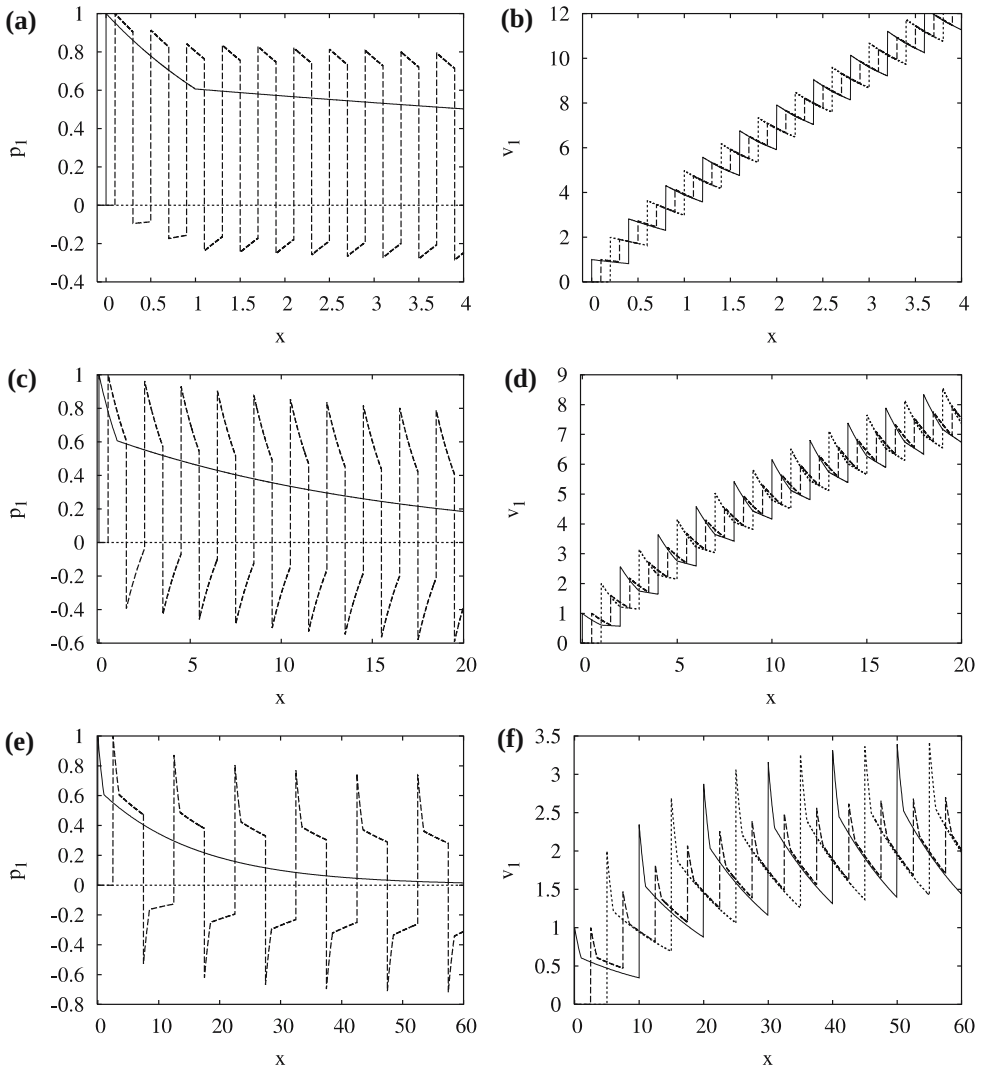

Figure 4. Profiles of p_1 and v_1 on $\psi = 0$ (solid lines), $\psi = h/2$ (dashed lines) and $\psi = h$ (dotted lines), for $C = 1$, $\alpha_1 = 0{\cdot}5$, $\alpha_2 = 0{\cdot}0625$ for (a) and (b) $h = 0{\cdot}2$, (c) and (d) $h = 1$ and (e) and (f) $h = 5$. (Supersonic case with free outer boundary).

Note that the terms on the right-hand side of Equations (35–38) correspond to a contribution to the solution from a point on the interface which is closer to the shock the higher the value of i. Since $p_I(x)$ is a monotonically decreasing function of x for $x > 0$, the terms corresponding to points closest to the shock will make the largest contribution to the solutions. For the even-numbered solution regions, it is the $i = n$ term which makes the largest contribution (note this makes a negative contribution to p_1 in these regions), while the $p_I(x - C\psi - 2nCh)$ term is largest in the odd-numbered-solution regions (note in both cases, these terms correspond to contributions from points on the interface within solution region 1).

Figure 4 shows the pressure and y-velocity perturbation profiles along $\psi = 0$, $h/2$ and h for inert thicknesses of $h = 0{\cdot}2$, 1 and 5, respectively, when $C = 1$, $\alpha_1 = 0{\cdot}5$ and $\alpha_2 = 0{\cdot}0625$. Figure 5 shows the profiles of y_I and y_h for these three inert thicknesses. Note first that v_1 and the interior profiles of p_1 jump at the boundaries between solution regions. As can be

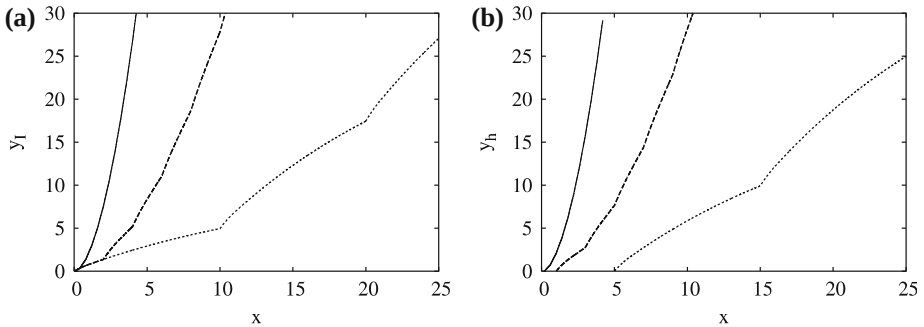

Figure 5. Profiles of (a) y_I (y_1 on $\psi = 0$) and (b) y_h (y_1 on $\psi = h$), for $C = 1$, $\alpha_1 = 0{\cdot}5$, $\alpha_2 = 0{\cdot}0625$ and $h = 0{\cdot}2$ (solid lines), $h = 1$ (dashed lines), $h = 5$ (dotted lines). (Supersonic case with free outer boundary).

seen in Figure 5, the slope in y_I and y_h are also discontinuous at the boundaries which follows from Equation (41). These 'reverberations' along the interface and outer edge of the inert are known as 'ringing'. The pressure is negative in the even-numbered-solution regions since the $-p_I(z + C\psi - 2nCh)$ term makes the largest contribution to p_1 in these regions. This indicates the inert is in tension here. In real materials, if the degree of tension is sufficiently large then spall will occur. It should also be noted that when the pressure becomes sufficiently low, material-strength effects will be quantitatively important [6]. However, these effects are not the focus of attention in this paper.

As h increases, the contribution to the solution of any given term with $i < n$ in Equations (35–38) comes from a point on the interface which moves further from the shock (corresponding to lower interface pressures), so that the contribution is smaller the larger the value of h. Hence the $i = n$ terms (corresponding to contributions from points on the interface in region 1) become increasingly dominant in the solution as the inert thickness is increased. One ramification of this can be seen in Figure 4. For larger h the minimum values of the pressure perturbation in the even-numbered-solution regions is lower since the positive terms in Equation (35) are smaller and hence have less of a balancing effect on the $-p_I(z + C\psi - 2nCh)$ term. Secondly, the increase in the local maximum values of v_1 (at the solution region boundaries) with region number, occurs more slowly for larger h. This is because the additional terms generated as one moves across the boundaries have a smaller contribution. Hence, as expected, the thinner the inert, the more rapidly the inert is deflected by the explosive (see Figure 5), and thus thinner inert layers will have less of a confining effect on the explosive.

Figure 6 shows p_1 and v_1 profiles for $h = 5$ but with $\alpha_2 = 0{\cdot}25$ and $\alpha_2 = 0{\cdot}5$ (note that the pressure release in the detonation products is more rapid for higher α_2). Figure 7 also shows the y-position perturbations of the edges of the confiner for the different α_2-values. Note that, as α_2 increases, and the pressure drops more rapidly along the interface in the region $x > 1$, the contributions from the $i < n$ terms in Equations (35–38) decrease and hence the contribution from the $i = n$ terms becomes more dominant. Thus, the degree of tension increases somewhat in the even-numbered-solution regions, indicating that spalling of the confiner is more likely with more rapid pressure releases. Also, the rate of overall increase in the v_1-values as one moves into subsequent regions decreases. Hence, the inert is deflected less rapidly. Note the ringing along the inert edges is more apparent for cases with a more rapid pressure release.

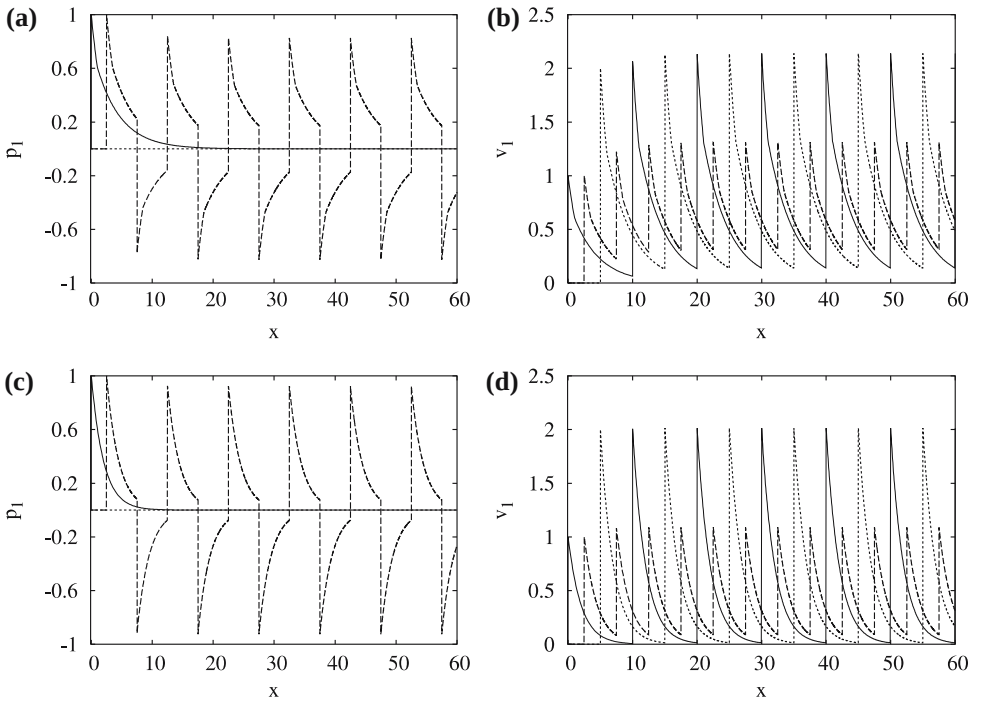

Figure 6. Profiles of p_1 and v_1 on $\psi = 0$ (solid lines), $\psi = h/2$ (dashed lines) and $\psi = h$ (dotted lines), for $C = 1$, $\alpha_1 = 0{\cdot}5$, $h = 5$ and (a) and (b) $\alpha_2 = 0{\cdot}25$, (c) and (d) $\alpha_2 = 0{\cdot}5$. (Supersonic case with free outer boundary).

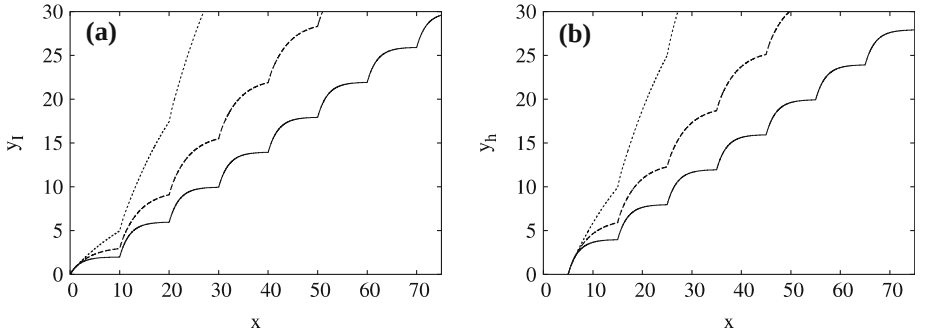

Figure 7. Profiles of (a) $y_I(y_1$ on $\psi = 0)$ and (b) $y_h(y_1$ on $\psi = h)$, for $C = 1$, $\alpha_1 = 0{\cdot}5$, $h = 5$ and $\alpha_2 = 0{\cdot}0625$ (dotted lines), $\alpha_2 = 0{\cdot}25$ (solid lines) and $\alpha_2 = 0{\cdot}5$ (dashed lines). (Supersonic case with free outer boundary).

3.2. Rigid-wall outer boundary

For the rigid-wall case, $v_h(x) = 0$, the method of characteristics yields for the solution in region 2

$$p_1(x, \psi) = p_I(x - C\psi) + p_I(x + C\psi - 2Ch), \tag{43}$$

$$v_1(x, \psi) = Cp_I(x - C\psi) - Cp_I(x + C\psi - 2Ch), \tag{44}$$

while the solution in region $2n$ $(n = 2, 3, 4, \ldots)$ is

$$p_1(x, \psi) = \sum_{i=0}^{n-1} (-1)^i p_I(x - C\psi - 2iCh) - \sum_{i=1}^{n} (-1)^i p_I(x + C\psi - 2iCh), \tag{45}$$

$$v_1(x,\psi)=C\sum_{i=0}^{n-1}(-1)^i p_I(x-C\psi-2iCh)+C\sum_{i=1}^{n}(-1)^i p_I(x+C\psi-2iCh), \tag{46}$$

and the solution in region $2n+1$ ($n=1,2,3,\ldots$) is

$$p_1(x,\psi)=\sum_{i=0}^{n}(-1)^i p_I(x-C\psi-2iCh)-\sum_{i=1}^{n}(-1)^i p_I(x+C\psi-2iCh), \tag{47}$$

$$v_1(x,\psi)=C\sum_{i=0}^{n}(-1)^i p_I(x-C\psi-2iCh)+C\sum_{i=1}^{n}(-1)^i p_I(x+C\psi-2iCh). \tag{48}$$

The interfacial-coupling condition is hence

$$v_I(x)=Cp_I(x)+2C\sum_{i=1}^{n}(-1)^i p_I(x-2iCh) \tag{49}$$

for $2nCh\le x\le(2n+2)Ch$, $n=1,2,3,\ldots$ Equation (49) is the principal result of this section.

Again, by prescribing the pressure along the interface, we can now solve for the deformation of the inert. Figure 8 shows the pressure and y-velocity perturbation profiles when the interface pressure is prescribed by Equation (42), while Figure 9 shows the resulting interface shapes. For the rigid outer boundary case, Figure 8 shows that the velocity of the interface alternates discontinuously from positive to negative values across the solution region boundaries. Hence, as can be seen in Figure 9, the interface is first deflected outwards by the pressure loading. However, the presence of the outer wall causes the interface to be subsequently deflected back in again, followed by further 'ringing' along the interface, with the deflection alternating directions. Note that for large x, the interface oscillates around the initial, undisturbed position, $y_I(x)=0$. These results for the interface shapes agree qualitatively well with those of the numerical simulations of confined explosive slabs in [2], which also used a rigid-wall boundary condition. Note also from Figure 9 that the amplitude of the oscillation decreases with decreasing inert thickness. Hence, in the first region behind the shock, the interface is initially deflected less far in the y-direction for thinner inerts. As expected, for the rigid-wall outer-boundary cases, the confinement effect on the detonation is enhanced as $h\to 0$.

Figure 8 also shows that again the interfacial pressure loading results in the interior of the inert consisting of alternating regions of compression and tension, including along the outer edge in this case.

4. Subsonic inert flow

For the case of subsonic flow in the inert (*e.g.*, for ANFO confined by copper corresponding to Figure 1c), Equations (21) are elliptic, and so the solution formally senses data from all four of the boundaries ($\psi=0$, $\psi=h$ and $x\to\pm\infty$). For this case, we subject the solution to the following boundary conditions:

1. p_1 and v_1 remain bounded as $x\to\pm\infty$;
2. p_1 is prescribed by $p_1=p_I(x)$ along $\psi=0$,
3. $p_1=0$ along $\psi=h$ (for the free outer boundary problem) or $v_1=0$ along $\psi=h$ (for the rigid-wall outer-boundary problem).

In this case we utilize the boundedness of p_1 and v_1 to seek the solution in terms of a Fourier transform of the form

$$p_1(\psi,x)=\int_{-\infty}^{\infty}C(\psi,k)\mathrm{e}^{-\mathrm{i}kx}\,\mathrm{d}k. \tag{50}$$

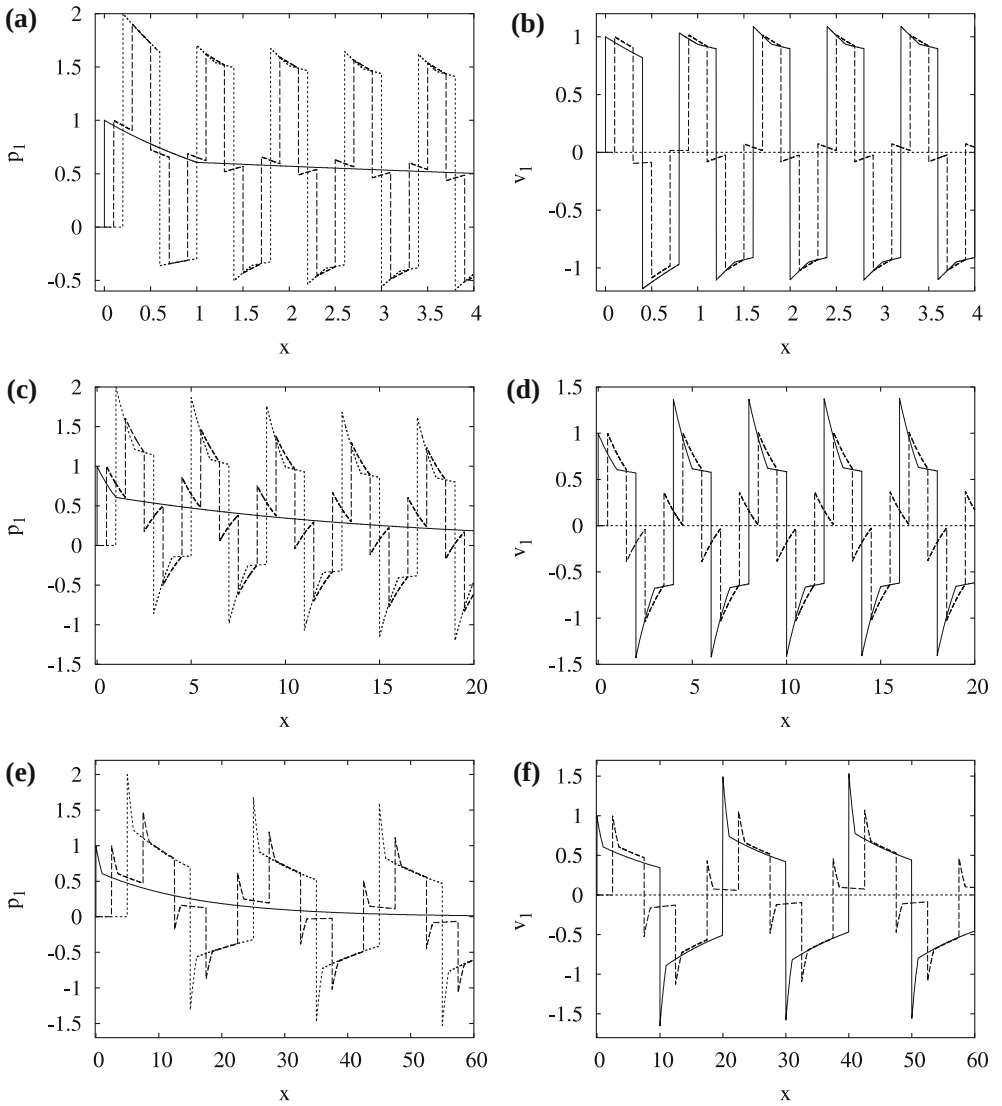

Figure 8. Profiles of p_1 and v_1 on $\psi = 0$ (solid lines), $\psi = h/2$ (dashed lines) and $\psi = h$ (dotted lines), for $C = 1$, $\alpha_1 = 0{\cdot}5$, $\alpha_2 = 0{\cdot}0625$ and (a) and (b) $h = 0{\cdot}2$, (c) and (d) $h = 1$ and (e) and (f) $h = 5$. (Supersonic case with rigid wall outer boundary).

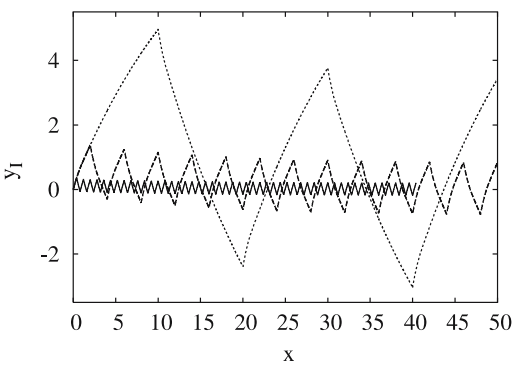

Figure 9. Profiles of $y_I(y_1 \text{ on } \psi = 0)$ for $C = 1$, $\alpha_1 = 0{\cdot}5$, $\alpha_2 = 0{\cdot}0625$ and $h = 0{\cdot}2$ (solid lines), $h = 1$ (dashed lines), $h = 5$ (dotted lines). (Supersonic case with rigid wall outer boundary).

Substituting Equation (50) in Equations (21) leads to the condition

$$\int_{-\infty}^{\infty}\left(\frac{\partial^2 C(\psi,k)}{\partial\psi^2}-\beta k^2 C(\psi,k)\right)\mathrm{e}^{-\mathrm{i}kx}\,\mathrm{d}k=0 \tag{51}$$

which the solution must satisfy.

4.1. Free-outer-boundary problem

For the free-boundary case, the nontrivial solution to Equation (51) which satisfies the boundary condition $p_1(h,x)=0$ requires

$$C(\psi,k)=\hat{C}(k)\frac{\sinh\left(kB(h-\psi)\right)}{\sinh\left(kBh\right)}, \tag{52}$$

where $B=\sqrt{\beta}$ and $\hat{C}(k)$ is set by requiring $p_1(0,x)=p_I(x)$, which on using the inverse transform yields

$$\hat{C}(k)=\frac{1}{2\pi}\int_{-\infty}^{\infty}p_I(x)\mathrm{e}^{\mathrm{i}kx}\,\mathrm{d}x. \tag{53}$$

Substituting Equation (52) in Equation (50) gives

$$p_1(\psi,x)=\frac{1}{2\pi}\int_{-\infty}^{\infty}\left(\int_{-\infty}^{\infty}p_I(x)\mathrm{e}^{\mathrm{i}k\hat{x}}\mathrm{d}\hat{x}\right)\frac{\sinh(kB(h-\psi))}{\sinh(kBh)}\mathrm{e}^{-\mathrm{i}kx}\,\mathrm{d}k. \tag{54}$$

Then substituting Equations (54) in Equations (51) gives

$$v_1(\psi,x)=\frac{iB}{2\pi}\int_{-\infty}^{\infty}\left(\int_{-\infty}^{\infty}p_I(\hat{x})\mathrm{e}^{\mathrm{i}k\hat{x}}\mathrm{d}\hat{x}\right)\frac{\cosh\left(kB(h-\psi)\right)}{\sinh\left(kBh\right)}\mathrm{e}^{-\mathrm{i}kx}\,\mathrm{d}k. \tag{55}$$

Equation (55) is the principal result of this section. It relates the deflection of the streamlines to the interface pressure, including the deflection of the interface itself by evaluation on $\psi=0$. Hence this equation evaluated on $\psi=0$ serves as the coupling condition between the explosive and inert.

To understand how the interface and the flow in the interior of the inert respond to the pressure loading, we can again prescribe the pressure along the interface. In particular, we examine what the two-stage-decay example with $p_I(x)$ given by Equation (42) predicts for the subsonic case. For this example, evaluating the Fourier transform of the pressure along the interface in Equation (53), we have

$$\int_{-\infty}^{\infty}p_I(\hat{x})\mathrm{e}^{\mathrm{i}k\hat{x}}\mathrm{d}\hat{x}=\frac{1-\exp(\mathrm{i}k-\alpha_1)}{\alpha_1-\mathrm{i}k}+\frac{\exp(\mathrm{i}k-\alpha_1)}{\alpha_2-\mathrm{i}k}. \tag{56}$$

The pressure in the interior of the inert is then

$$\begin{aligned}p_1(\psi,x)=\frac{1}{2\pi}\int_{-\infty}^{\infty}&\left(\frac{\exp(-\mathrm{i}kx)-\exp(-\mathrm{i}k(x-1)-\alpha_1)}{\alpha_1-\mathrm{i}k}+\frac{\exp(-\mathrm{i}k(x-1)-\alpha_1)}{\alpha_2-\mathrm{i}k}\right)\\&\times\frac{\sinh\left(kB(h-\psi)\right)}{\sinh\left(kBh\right)}\mathrm{d}k.\end{aligned} \tag{57}$$

We can evaluate this integral by using contour integration and the Cauchy integral formula of complex variable calculus, with k considered to be a complex variable. After some analysis, one finds that

$$p_1(\psi,x)=\begin{cases}p_{1a}(\psi,x) & x<0,\\ p_{1b}(\psi,x) & 0\le x\le 1\\ p_{1c}(\psi,x) & x>1,\end{cases}, \tag{58}$$

where

$$p_{1a}(\psi,x)=-\sum_{n=1}^{\infty}(-1)^n\frac{\exp(n\pi x/Bh)}{(\alpha_1 Bh+n\pi)}\sin(n\pi(1-\psi/h))$$
$$-(\alpha_1-\alpha_2)Bh\sum_{n=1}^{\infty}(-1)^n\frac{\exp(-\alpha_1+n\pi(x-1)/Bh)}{(\alpha_1 Bh+n\pi)(\alpha_2 Bh+n\pi)}\sin(n\pi(1-\psi/h)), \tag{59}$$

$$p_{1b}(\psi,x)=\exp(-\alpha_1 x)\frac{\sin(\alpha_1 B(h-\psi))}{\sin(\alpha_1 Bh)}$$
$$-\sum_{n=1}^{\infty}(-1)^n\frac{\exp(-n\pi x/Bh)}{(\alpha_1 Bh-n\pi)}\sin(n\pi(1-\psi/h))$$
$$-(\alpha_1-\alpha_2)Bh\sum_{n=1}^{\infty}(-1)^n\frac{\exp(-\alpha_1+n\pi(x-1)/Bh)}{(\alpha_1 Bh+n\pi)(\alpha_2 Bh+n\pi)}\sin(n\pi(1-\psi/h)), \tag{60}$$

$$p_{1c}(\psi,x)=\exp(-\alpha_2 x-(\alpha_1-\alpha_2))\frac{\sin(\alpha_2 B(h-\psi))}{\sin(\alpha_2 Bh)}$$
$$-2\pi\sum_{n=1}^{\infty}(-1)^n\frac{\exp(-n\pi x/Bh)}{(\alpha_1 Bh-n\pi)}\sin(n\pi(1-\psi/h))$$
$$-(\alpha_1-\alpha_2)Bh\sum_{n=1}^{\infty}(-1)^n\frac{\exp(-\alpha_1-n\pi(x-1)/Bh)}{(\alpha_1 Bh-n\pi)(\alpha_2 Bh-n\pi)}\sin(n\pi(1-\psi/h)). \tag{61}$$

Again, using complex contour integration to determine the integral in Equation (55), we also obtain

$$v_1(\psi,x)=\begin{cases} v_{1a}(\psi,x) & x<0,\\ v_{1b}(\psi,x) & 0\le x\le 1,\\ v_{1c}(\psi,x) & x>1,\end{cases} \tag{62}$$

where

$$v_{1a}(\psi,x)=-B\sum_{n=1}^{\infty}(-1)^n\frac{\exp(n\pi x/Bh)}{(\alpha_1 Bh+n\pi)}\cos(n\pi(1-\psi/h))$$
$$-(\alpha_1-\alpha_2)\beta h\sum_{n=1}^{\infty}(-1)^n\frac{\exp(-\alpha_1+n\pi(x-1)/Bh)}{(\alpha_1 Bh+n\pi)(\alpha_2 Bh+n\pi)}\cos(n\pi(1-\psi/h)), \tag{63}$$

$$v_{1b}(\psi,x)=\frac{1}{\alpha_1 h}-B\exp(-\alpha_1 x)\frac{\cos(\alpha_1 B(h-\psi))}{\sin(\alpha_1 Bh)}$$
$$+B\sum_{n=1}^{\infty}(-1)^n\frac{\exp(-n\pi x/Bh)}{(\alpha_1 Bh-n\pi)}\cos(n\pi(1-\psi/h))$$
$$-(\alpha_1-\alpha_2)\beta h\sum_{n=1}^{\infty}(-1)^n\frac{\exp(-\alpha_1+n\pi(x-1)/Bh)}{(\alpha_1 Bh+n\pi)(\alpha_2 Bh+n\pi)}\cos(n\pi(1-\psi/h)), \tag{64}$$

$$v_{1c}(\psi, x) = \frac{1}{\alpha_1 h} + \frac{1}{h}\left(\frac{1}{\alpha_2} - \frac{1}{\alpha_1}\right)\exp(-\alpha_1)$$
$$-B\exp(-\alpha_2 x - (\alpha_1 - \alpha_2))\frac{\cos(\alpha_2 B(h-\psi))}{\sin(\alpha_2 Bh)}$$
$$+B\sum_{n=1}^{\infty}(-1)^n\frac{\exp(-n\pi x/Bh)}{(\alpha_1 Bh - n\pi)}\cos(n\pi(1-\psi/h))$$
$$+(\alpha_1-\alpha_2)\beta h\sum_{n=1}^{\infty}(-1)^n\frac{\exp(-\alpha_1 - n\pi(x-1)/Bh)}{(\alpha_1 Bh - n\pi)(\alpha_2 Bh - n\pi)}\cos(n\pi(1-\psi/h)). \quad (65)$$

The streamline shapes, including the interface and outer edge of the inert, can be straightforwardly obtained by integrating Equation (62) with respect to x for constant ψ.

Figure 10 shows profiles of p_1 and v_1 along different streamlines for $B = 0{\cdot}5$, $\alpha_1 = 0{\cdot}5$, $\alpha_2 = 0{\cdot}0625$ and inert thicknesses of $h = 0{\cdot}2$, 1 and 5. Figure 11 shows the shapes of the explosive-inert interface and the outer edge of the inert for these parameters and values of h. Also shown in Figure 11(c) are interior streamline shapes for $h = 5$.

Note first from Figure 10 that although there is a discontinuity in the pressure along the interface, the flow in the interior of the confiner is smooth, albeit with rapid changes in the interior pressure near the origin. As the inert thickness increases, these rapid changes in pressure also become more diffuse as one approaches the outer edge. The y-velocity on the interface has a negative spike at $x = 0$, indicating that the interface is initially deflected *into* the explosive, as can be seen to be the case in Figure 11(a). The width of the spike increases with h. Thus, with increasing h, the inert is deflected further into the explosive and over a larger region (see Figures 11a and 12a). However, Figure 10 also shows that away from the origin, the y-velocities become independent of ψ. So for large enough x, the streamlines all become parallel, as can be seen in Figure 11(c). Figure 11(b) shows that the y-position of the outer edge of the confiner increases monotonically with x. As for the supersonic case, the interface is deflected more rapidly for thinner inerts. Thus, as h decreases, the inert will have less of a confining effect on the detonation.

Figure 12 shows the interface shape for various values of h and B. Figure 12(a) shows that as h increases for B fixed, the interface continues to be deflected further and further into the explosive, and over a larger distance. In the limit of infinite confiner thickness, formally the inert would provide compression of the interior of the explosive ahead of the shock, which could lead to an increase in the detonation speed. Figure 12(b) gives the interface shape for various values of B, with h fixed but large, which shows that as B decreases the interface deflection into the explosive becomes less pronounced (note, however, that formally as $B \to 0$ nonlinear effects must be re-instated as the flow becomes of the transonic type; see Section 5). The results in Figure 12 hence are suggestive that, for large confiner thicknesses, if the pressure profile along the interface is to be of the form of a lead shock followed by a decaying pressure, the detonation speed would not be able to drop below the ambient sound speed of the inert. Alternatively, the assumption that the pressure on the interface ahead of the detonation shock is undisturbed may break down for large h, in that the inert may drive a precursor wave ahead of the detonation shock in the explosive. Indeed, Eden and Belcher [8] performed experiments on slabs of the explosive EDC35, confined on one side by brass and the other by beryllium. Their results indicate that, on the beryllium side of the explosive, a compression wave in the beryllium drives a shock in the explosive ahead of the detonation wave. This is somewhat akin to what happens at fast-slow interfaces in gases [9]. However, in our subsonic inert-flow case, we do not expect a shock in the confiner when steady state is achieved.

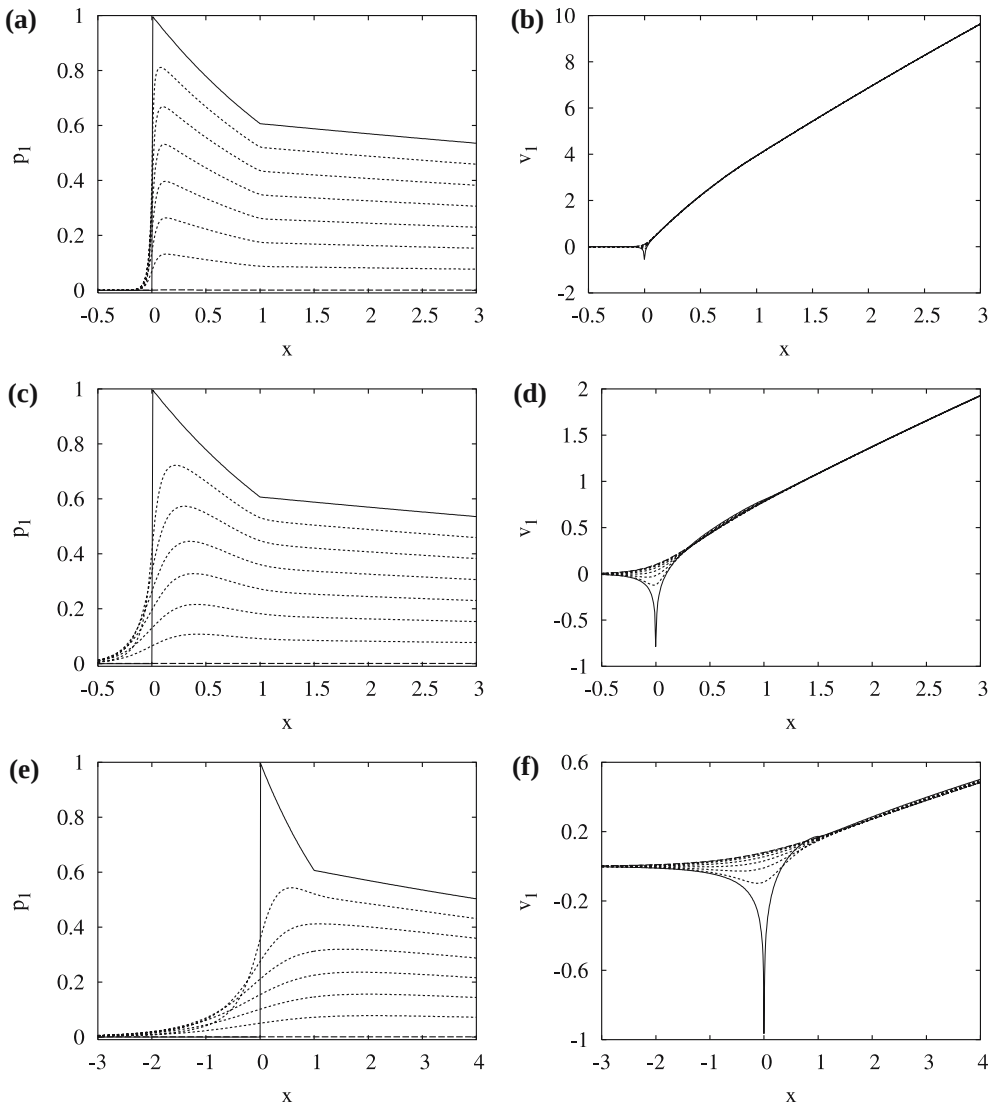

Figure 10. Profiles of p_1 and v_1 on $\psi = 0$ (solid lines), $\psi = h$ (dashed lines) and six equally spaced intermediate values of ψ (dotted lines), for $B = 0{\cdot}5$, $\alpha_1 = 0{\cdot}5$, $\alpha_2 = 0{\cdot}0625$ and (a) and (b) $h = 0{\cdot}2$, (c) and (d) $h = 1$ and (e) and (f) $h = 5$.

Figure 13 shows the effect of more rapid pressure releases, *i.e.*, profiles of p_1 and v_1 for $\alpha_2 = 0{\cdot}25$ and $\alpha_2 = 0{\cdot}5$, when $B = 0{\cdot}5$, $\alpha_1 = 0{\cdot}5$ and $h = 5$. Figure 14 also shows the interface and outer-edge streamline shapes for various values of α_2. The p_1 and v_1 profiles for different rates of pressure release are qualitatively similar, with the more rapid pressure decay along the interface reflected in more rapid decays along the interior streamlines (Figure 13a and b), while the profiles of v_1 along different streamlines become somewhat more spread out for $x > 0$. Figure 14 shows that the pressure release rate has very little effect on the region of the interface deflected into the inert or the outer edge shape near $x = 0$. For larger x, the interface and outer edge shapes do begin to diverge more, with more rapid pressure releases (larger α_2) producing smaller deflections of the inert at a given x-position.

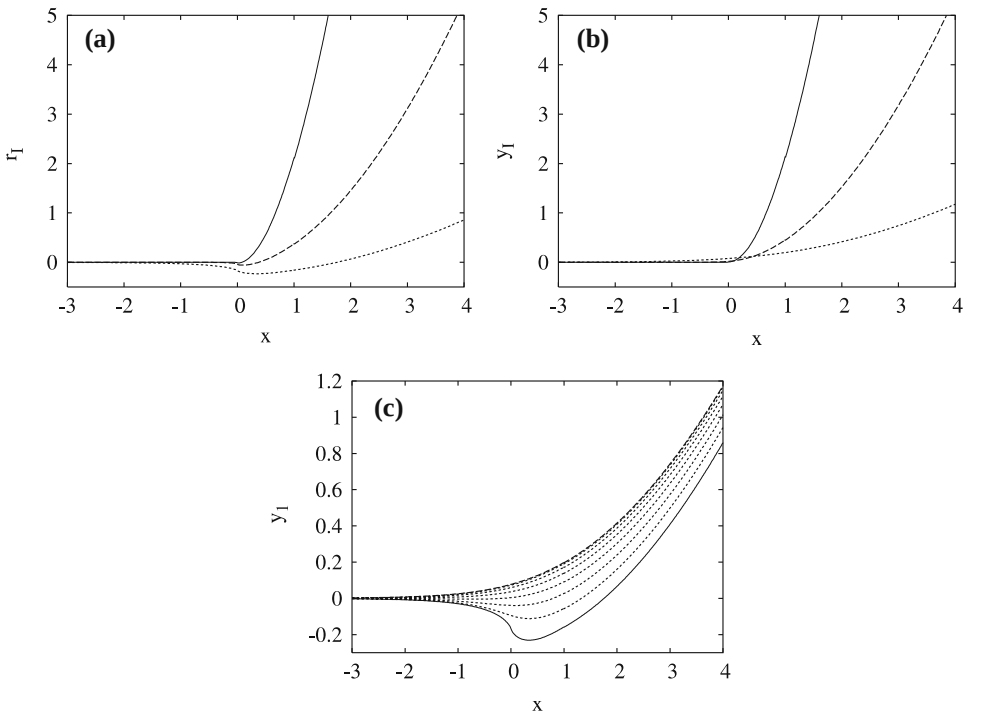

Figure 11. Profiles of (a) $y_I(y_1$ on $\psi = 0)$ and (b) $y_h(y_1$ on $\psi = h)$ for $B = 0{\cdot}5$, $\alpha_1 = 0{\cdot}5$, $\alpha_2 = 0{\cdot}0625$ and $h = 0{\cdot}2$ (solid lines), $h = 1$ (dashed lines), $h = 5$ (dotted lines), and (c) y_1 on eight equally spaced values of ψ from $\psi = 0$ to $\psi = h$ for $h = 5$. (Subsonic case with free outer boundary).

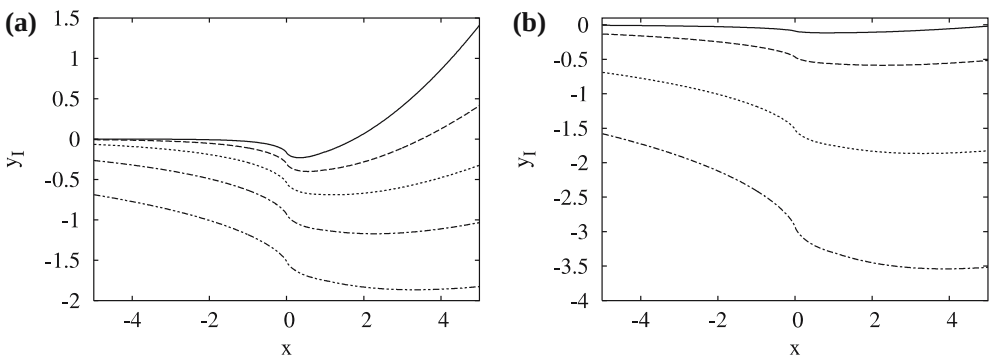

Figure 12. Profiles of y_I for $\alpha_1 = 0{\cdot}5$, $\alpha_2 = 0{\cdot}0625$ and (a) $B = 0{\cdot}5$ and $h = 5$ (solid line), 10 (dashed line), 20 (dotted line), 40 (dot-dashed line) and 80 (double-dot-dashed line), and (b) $h = 80$ and $B = 0{\cdot}1$ (solid line), 0·25 (dashed line), 0·5 (dotted line) and 0·75 (dot-dashed line). (Subsonic case with free outer boundary).

4.2. Rigid-wall outer boundary

The nontrivial solution to Equation (51) which satisfies $p_1(0, x) = p_I(x)$ and $v(h, x) = v_h(x) = 0$ is

$$C(\psi, k) = \hat{C}(k) \frac{\cosh(kB(h - \psi))}{\cosh(kBh)}, \tag{66}$$

where again $\hat{C}(k)$ is set by the pressure loading along $\psi = 0$ by Equation (53). In this case, the pressure and y-velocity are hence

$$p_1(\psi, x) = \frac{1}{2\pi} \int_{-\infty}^{\infty} \left(\int_{-\infty}^{\infty} p_I(x) e^{ik\hat{x}} d\hat{x} \right) \frac{\cosh(kB(h-\psi))}{\cosh(kBh)} e^{-ikx} dk, \tag{67}$$

and

$$v_1(\psi, x) = \frac{iB}{2\pi} \int_{-\infty}^{\infty} \left(\int_{-\infty}^{\infty} p_I(\hat{x}) e^{ik\hat{x}} d\hat{x} \right) \frac{\sinh(kB(h-\psi))}{\cosh(kBh)} e^{-ikx} dk. \tag{68}$$

Equation (68) evaluated on $\psi = 0$ is the principal result.

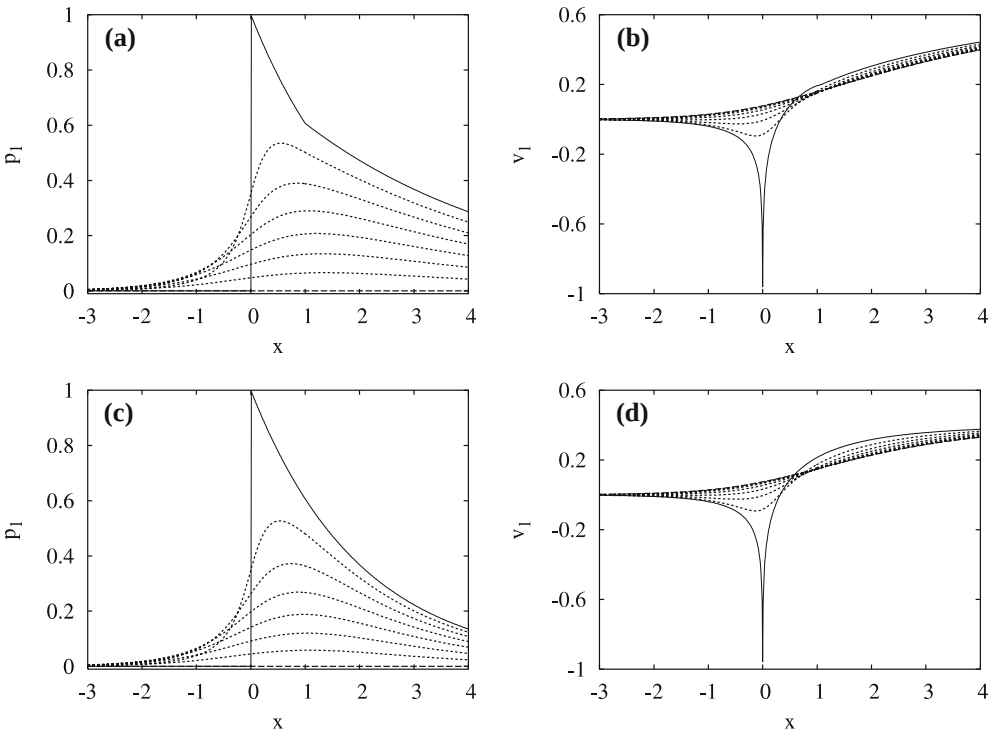

Figure 13. Profiles of p_1 and v_1 on $\psi = 0$ (solid lines), $\psi = h$ (dashed lines) and six equally spaced intermediate values of ψ (dotted lines), for $B = 0{\cdot}5$, $\alpha_1 = 0{\cdot}5$, $h = 5$ and (a) and (b) $\alpha_2 = 0{\cdot}25$ and (c) and (d) $\alpha_2 = 0{\cdot}5$. (Subsonic case with free outer boundary).

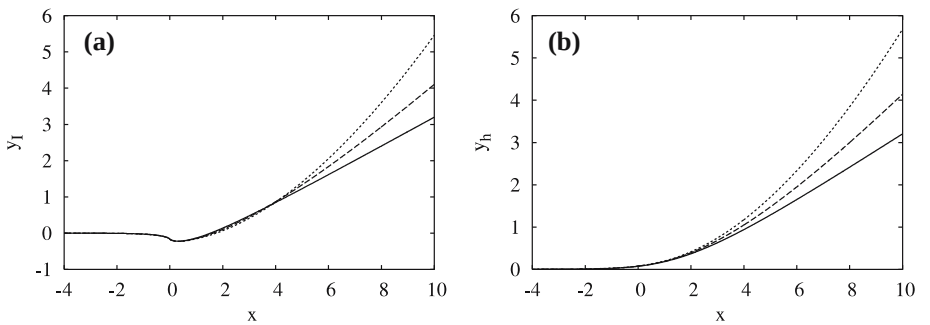

Figure 14. Profiles of (a) y_I (y_1 on $\psi = 0$) and (b) y_h (y_1 on $\psi = h$) for $B = 0{\cdot}5$, $\alpha_1 = 0{\cdot}5$, $h = 5$ and $\alpha_2 = 0{\cdot}5$ (solid lines), $\alpha_2 = 0{\cdot}25$ (dashed lines) and $\alpha_2 = 0{\cdot}0625$ (dotted lines). (Subsonic case with free outer boundary).

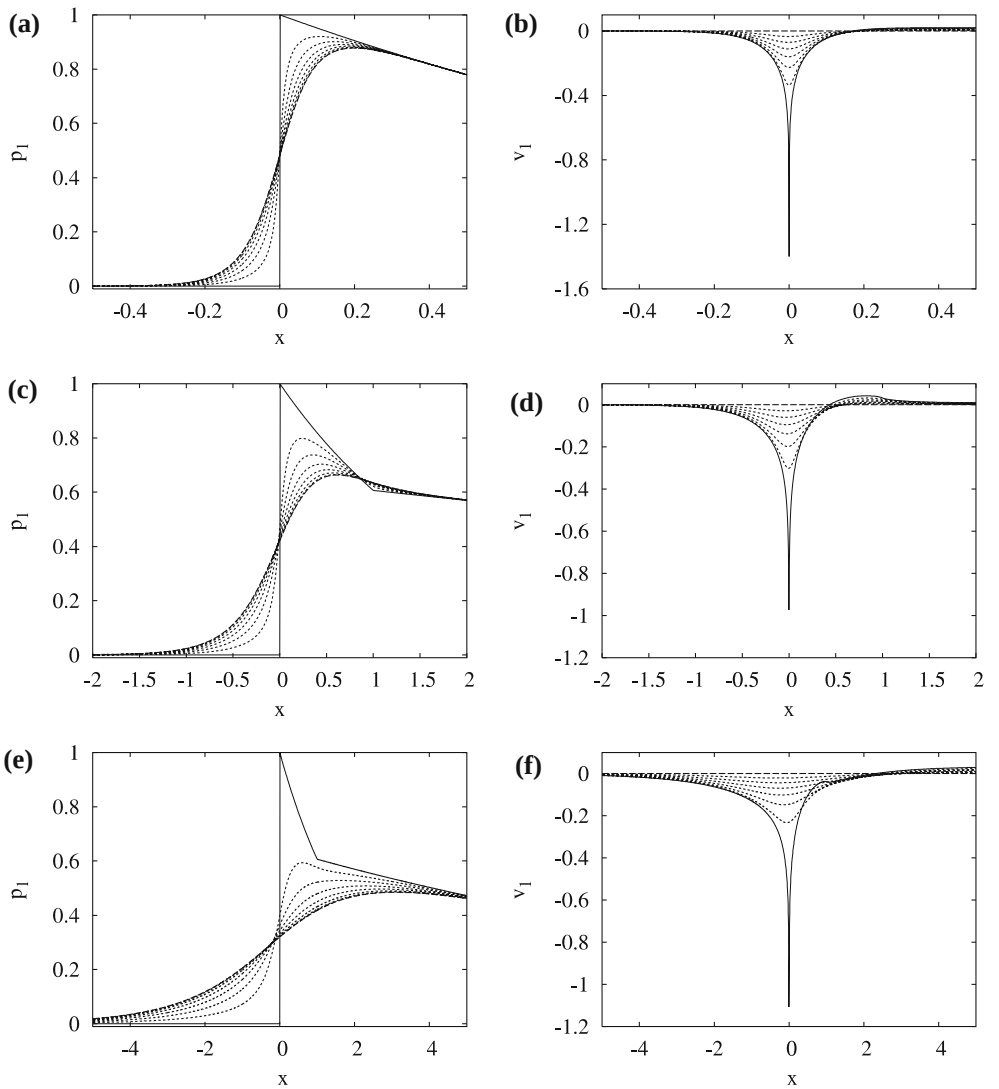

Figure 15. Profiles of p_1 and v_1 on $\psi = 0$ (solid lines), $\psi = h$ (dashed lines) and six equally spaced intermediate values of ψ (dotted lines), for $B = 0{\cdot}5$, $\alpha_1 = 0{\cdot}5$, $\alpha_2 = 0{\cdot}0625$ and (a) and (b) $h = 0{\cdot}2$, (c) and (d) $h = 1$ and (e) and (f) $h = 5$. (Subsonic case with rigid wall outer boundary).

Let us once more see how the solution in the inert behaves if the pressure loading along the interface is prescribed by the form in Equation (42). Figure 15 shows profiles of p_1 and v_1 in the inert for various inert thickness, while Figure 16(a) shows the interface shapes for these cases, and Figure 16(b) shows the perturbation to the streamline shapes in the interior for $h = 5$. Figure 15 shows that in this case the pressure sufficiently far downstream becomes independent of ψ, and that the pressure along the outer wall is a diffuse form of the interface profile (the larger h, the more diffused the pressure profile becomes at the outer edge).

Figure 15 also shows that again there is a negative spike in v_1 along the interface, so that, as for the free-boundary case, the inert is initially deflected towards the explosive (Figure 16). Subsequent to the spike, v_I becomes positive and then asymptotes back to zero, so that the interface begins to move back out again. For sufficiently large values of x, v_1 tends to zero on all the streamlines, and Figure 16(b) shows that the confiner returns to its

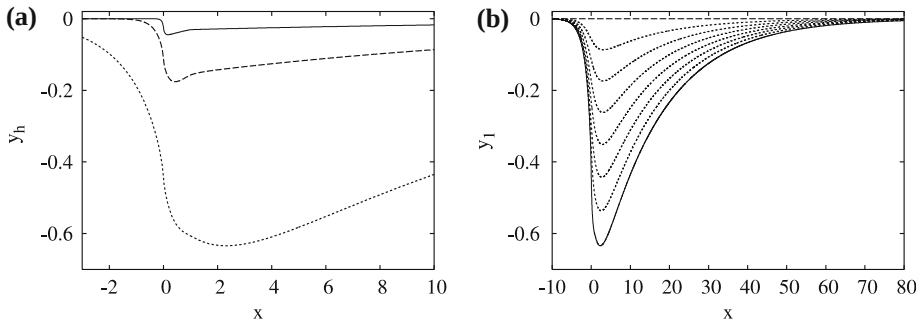

Figure 16. Profiles of (a) y_I (y_1 on $\psi = 0$) for $B = 0{\cdot}5$, $\alpha_1 = 0{\cdot}5$, $\alpha_2 = 0{\cdot}0625$ and $h = 0{\cdot}2$ (solid lines), $h = 1$ (dashed lines), $h = 5$ (dotted lines), and (b) y_1 on eight equally spaced values of ψ from $\psi = 0$ to $\psi = h$ for $h = 5$. (Subsonic case with rigid wall outer boundary).

undisturbed position. Hence in this case, the entire deflected portion of the interface is pushed into the explosive ($y_I(x) \leq 0$ everywhere). Note also that, for a given value of h, the inert is deflected much further into the explosive side of the undisturbed interface position for the rigid-wall case than for the free-boundary case. Again, however, for fixed h, the deflection is smaller as $B \to 0$. Thus, as for the free-boundary case, these results suggest that for sufficiently large h, the deflection of the inert will drive the detonation speed up to near the confiner sound speed or drive a precursor wave ahead of the detonation in the explosive.

5. Transonic inert flows

In this section we briefly consider intermediate cases where the initial inert sound speed is close to the detonation speed in the explosive. These cases lead to transonic flows in which nonlinearity is reinstated.

Consider the case where the initial sound speed in the inert is given by $c^2 = 1 + A\delta$ for some constant A, *i.e.*, the sound speed is within $O(\delta)$ of the explosive detonation speed, where δ is still the scaled shock-match pressure. For such a case, we are led to expansions of the form (cf [10, pp. 46–60]),

$$\begin{aligned} &p = \delta p_1 + \delta^2 p_2 + O(\delta^3), \quad \rho = 1 + \delta\rho_1 + \delta^2\rho_2 + O(\delta^3), \quad u = 1 + \delta u_1 + \delta^2 u_2 + O(\delta^3), \\ &v = \delta^{3/2} v_{3/2} + O(\delta^{5/2}), \quad \theta = \delta^{3/2}\theta_{3/2} + O(\delta^{5/2}), \quad c^2 = 1 + \delta c_1^2 + O(\delta^2), \\ &\psi = \delta^{\nu}\psi_{\nu}, \quad x = \delta^{\mu} x_{\mu}, \quad y = \delta^{\nu}\psi + \delta^{\nu+2} y_{\nu+2} + o\left(\delta^{\nu+2}\right), \quad 2\mu - 2\nu = 1. \end{aligned} \tag{69}$$

The selection for the scalings of the independent variables, μ and $\nu = \mu - 1/2$, will in general be problem dependent [10]. They may, for example, be selected by the choice of h in our inert confinement problem. Furthermore, there may be a number of different scalings needed in different regions for any given problem.

Taylor expanding the internal energy gives

$$e(p, \rho) = e_i + (e_{pi} p_1 + e_{\rho i}\rho_1)\delta + \left(\frac{1}{2} e_{ppi} p_1^2 + e_{p\rho i} p_1\rho_1 + \frac{1}{2} e_{\rho\rho i}\rho_1^2 + e_{pi} p_2 + e_{\rho i}\rho_2\right)\delta^2 + \cdots \tag{70}$$

Here an 'i' subscript denotes values in the initial quiescent inert state (where $p=0,\ \rho=1$), and

$$e_i = e(0,1), \quad e_{pi} = \left(\frac{\partial e}{\partial p}\right)_{(p=0,\rho=1)}, \quad e_{ppi} = \left(\frac{\partial^2 e}{\partial p^2}\right)_{(p=0,\rho=1)}, \tag{71}$$

etc. However, since $c_i^2 = 1 + A\delta$, the internal energy at the initial state will also have an asymptotic expansion, *i.e.*,

$$e_i = e(0,1) = e_{i0} + \delta e_{i1} + \cdots \tag{72}$$

For example, for a simple Tait equation of state with $e = (p + an)/((n-1)\rho)$ and $c^2 = (np + an)/\rho$, then the transonic case would require $c_i^2 = an = 1 + A\delta$, and hence $e_i = an/(n-1) = 1/(n-1) + \delta A/(n-1)$. Similarly quantities like e_{pi} will also have their expansions. In particular, evaluating Equation (2) in the initial state gives

$$e_{\rho i0} = -e_{pi0}, \quad e_{\rho i1} = -(Ae_{pi0} + e_{pi1}). \tag{73}$$

Hence the complete expansion for the internal energy is

$$e(p,\rho) = e_{i0} + (e_{i1} + e_{pi0}(p_1 - \rho_1))\delta + \left(e_{i2} + e_{pi1}p_1 - (e_{pi1} + Ae_{pi0})\rho_1 + \frac{1}{2}e_{ppi0}p_1^2 + e_{p\rho i0}p_1\rho_1 + \frac{1}{2}e_{\rho\rho i0}\rho_1^2 + e_{pi0}(p_2 - \rho_2)\right)\delta^2 + O(\delta^3). \tag{74}$$

Substitution in the Bernoulli Equation (3), together with the integration of Equation (2) along an isentrope, gives

$$\rho_1 = p_1, \quad \rho_2 = p_2 - p_1(a_1 p_1 + A), \quad u_1 = -p_1, \quad u_2 = -p_2, \tag{75}$$

where

$$a_1 = \frac{1}{2e_{pi0}}\left(1 - e_{ppi0} - e_{\rho\rho 0} - 2e_{p\rho i0}\right). \tag{76}$$

Hence $(\rho u)^{-1} = 1 + O(\delta^2)$.

The governing Equations (1) then give the nonlinear leading-order equations:

$$\frac{\partial^2 y_{v+2}}{\partial \psi_v^2} + \eta_1 \frac{\partial^2 y_{v+2}}{\partial {x_\mu}^2} = 0, \quad p_1(a_2 p_1 + A) = \frac{\partial y_{v+2}}{\partial \psi_v}, \tag{77}$$

where

$$a_2 = a_1 + 1, \quad \eta_1 = 2a_2 p_1 + A \tag{78}$$

and $\eta = c^2 - (u^2 + v^2) = \delta\eta_1 + O(\delta^2)$ is the sonic parameter. Hence Equation (77) is hyperbolic in regions of supersonic flow where $\eta_1 < 0$ or $p_1 < -A/(2a_2)$, elliptic in subsonic regions where $\eta_1 > 0$ or $p_1 > A/(2a_2)$ and parabolic on sonic loci where $\eta_1 = 0$.

In this case we cannot write down an explicit coupling condition between the explosive and inert, *i.e.*, a condition relating p_1 and v_1 (or θ_1) along the interface, since the nonlinear, mixed-type Equation (77) would require numerical solution, *e.g.*, using the methods in [11], which we do not attempt here, especially since the results would depend on the choice of form and parameters of the equation of state (*e.g.*, for the Tait eos example, $a_2 = (n+1)/2$). Hence the principal result of this section are the transonic scalings (70), which show that in these cases the deflection of the inert is higher order than for the $\beta = O(1)$ cases, since

$\theta = v = O(\delta^{3/2})$ when $\beta = O(\delta)$. Thus, we find that for either subsonic or supersonic flow, as the inflow speed approaches sonic values (the detonation speed approaches the initial sound speed of the inert) the confinement affect of the inert on the detonation is enhanced.

It is still also worth qualitatively classifying the types of flows one may expect for the transonic case. For supersonic inflow, $A < 0$, the detonation will still drive a shock into the inert. In this case, the shock jump conditions give, on the leading-order shock locus $x = x_s(\psi)$,

$$\begin{aligned} &\phi = \delta^{1/2}\phi_1 + O(\delta^{3/2}), \quad \rho_s = 1 + \delta p_{1s} + \delta^2(p_{2s} + p_{1s}(\phi_1^2 + p_{1s})) + O(\delta^3), \\ &u_s = 1 - \delta p_{1s} - \delta^2 p_{2s} + O(\delta^3), \quad v_s = \theta_s = \delta^{3/2}\phi_1 p_{1s} + O(\delta^{3/2}), \end{aligned} \tag{79}$$

where $\phi(\psi)$ is the angle the shock normal makes with the x-direction at a point on the shock locus, and

$$\phi_1 = (-a_2 p_{1s} + |A|)^{1/2}. \tag{80}$$

Hence for the transonic case, the leading-order shock locus is no longer a straight line, but the local shock angle depends on the local value of p_{1s}, while the shock normal angle is smaller, only $O(\delta^{1/2})$ compared to $O(1)$ for the $\beta = O(1)$ case considered in Section 3. Thus for transonic flows, the shock is more nearly normal to the inflow. Equation (80) shows that the shock is normal to the inflow ($\phi_1 = 0$) when $p_{1s} = |A|/a_2$, and hence this is the maximum possible shock pressure. Note also that Equations (80) were used to determine that the constant of integration of Equation (2) along a isentrope behind the shock is zero everywhere, up to and including $O(\delta^2)$, for the supersonic case ($A < 0$).

Since the shock is more nearly normal in the transonic case, it is hence possible to have subsonic post-shock states, which would require, $p_{1s} > |A|/(2a_2)$ by Equation (78). For example for the post-shock state to be subsonic at the interface, *i.e.*, at $\psi = z = 0$ where $p_{1s} = 1$, we require $|A| < 2a_2$. This case would hence correspond to the type of shock polar match shown in Figure 1(c). More generally for the flow at any point in the inert to be locally subsonic requires $p_1 > |A|/(2a_2)$, *i.e.*, the pressure needs to be sufficiently large. Assuming a case where we have subsonic post-shock flow at the interface and that the pressure profile along the interface behind the shock is a decaying one, then the flow on the interface would become supersonic once the interface pressure dropped below $|A|/(2a_2)$. Hence, for these types of shock polar matches (subsonic post-shock states in both the explosive and inert) one would only expect a small pocket of subsonic flow to exist in the inert in a region behind the shock and adjacent to the interface.

For subsonic inflows, $A > 0$. Thus, for the flow to become locally supersonic anywhere in the inert, the pressure would have to become sufficiently large and negative (hence the inert would have to be under sufficient tension), the requirement being $p_1 < -2a_2 A$. When the pressure is assumed to remain greater than this everywhere, Equation (77) would be a nonlinear equation of elliptic type in the inert, so that the interior flow would be smooth. This is the situation which we would expect to occur, for example, in the realistic case that the pressure along the interface was nonnegative everywhere.

Given our findings for the subsonic cases considered in Section 4 that suggest for very thick inerts the detonation in the explosive may be driven up to the sound speed of the inert, a special case of interest of the above is sonic inflow, or $A = 0$. In this case, sonic conditions are obtained when $p_1 = 0$, with supersonic flow only when $p_1 < 0$. If nonnegative pressure is assumed everywhere, Equation (77) would be elliptic (and hence the flow shockless) in the interior but parabolic on sonic loci where $p_1 = 0$, corresponding to $x \to 0$ and to $\psi = h$ for the free-boundary problem.

6. Conclusions

In this paper we have used the asymptotic limit of small disturbances in a strong inert confiner to obtain coupling conditions between a detonation running in an adjacent explosive and the deformation of the inert (confinement effect), in terms of relationships between the pressure and the interfacial deflection along the explosive-inert interface. The relationship was determined for cases where the detonation speed in the explosive was greater than or less than the ambient sound speed of the inert (subsonic and supersonic inert flow, respectively). Although the complete solution in the explosive and inert is a highly coupled problem, by prescribing the pressure along the interface with qualitatively expected explosive profiles, we then used the coupling conditions to solve for the leading-order solution everywhere in the inert in order to determine the qualitative effects of detonations on inert confiners of finite thickness, and how the supersonic and subsonic cases dramatically differ.

Transonic flows, where the detonation speed is close to the sound speed of the inert were also considered, but an explicit coupling condition cannot be determined in such cases due to the complex nonlinear, mixed type nature of the resulting leading-order equations. However, the analysis showed that for either the subsonic or supersonic cases, as the detonation speed approaches the ambient sound speed of the inert, the confinement effect of the inert on the detonation is increased in that the flow deflection angle becomes of smaller order.

The interfacial coupling condition provides the necessary information to solve the complete coupled problem of a confined steady detonation in an explosive, under the DSD weak curvature approximations for the outer region of the detonation and the small induced disturbance approximations in the inert confiner. Such a study, solving for the DSD explosive region, explosive inner boundary layers adjacent to the interface and the flow in the inert is currently underway.

We also intend to perform fully nonlinear, multi-material numerical simulations of the problem, and to compare with the asymptotic analysis. However, for these types of problems the interface typically needs to be numerically 'tracked' in some way and kept sharp in the numerical solution (instead of allowing the interface to smear out via inherent numerical viscosity), especially when the equation of state model for the inert is markedly different to that in the explosive. While a number of tracking algorithms exist, the applicability and numerical issues involved with the different algorithms for these types of reactive-inert interface problems do not appear to have been properly studied (indeed 'closure' issues are known to exist). Hence it would first be worth properly examining and understanding the strengths and weaknesses of various tracking schemes when applied to such problems.

The asymptotic limit employed in this paper, namely small scaled pressures or small overall change of the sound speed in the inert, is valid for sufficiently strong inerts or sufficiently weak explosives. However, it is also worth noting here that other interesting types of interactions are possible between weak explosives and weak confiners. Figure 17 shows theoretical shock polars for cardboard and porous ANFO, running at shock speed, $D_0 = 5{\cdot}2$ and $4{\cdot}0$ km/s. For this explosive-inert confiner pair, Figure 17 shows that the shock polars for the two material almost overlay over a wide region, and this behavior persists for a large range of detonation speeds. Interestingly, experiments by Catanach and Hill [12] and Bdzil *et al.* [13] found very different matches in terms of the measured shock normal angles at the edge of the explosive for this explosive-inert pair and for two different lots of ANFO: Catanach and Hill [12] found edge-shock angles of around 50° (this lot had experienced some separation and had a reduced fuel oil content), while Bdzil *et al.*'s [13] results gave edge angles of around 25–29°. The near overlay of the shock polars seen in Figure 17 explains why a unique and consistent

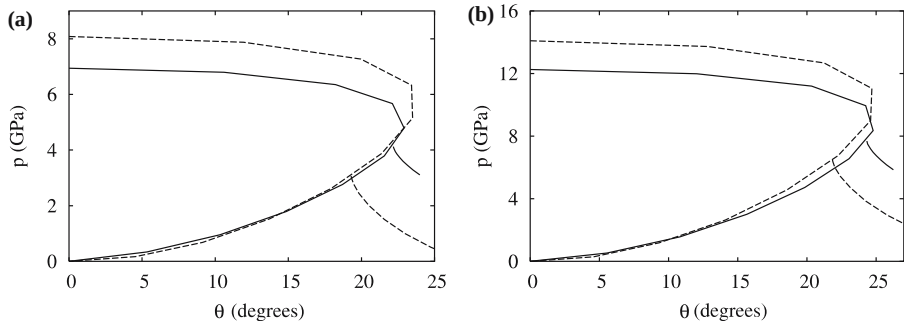

Figure 17. (a) Shock polars (shock pressure against streamline deflection angle) for cardboard (solid lines) and ANFO (dashed line) running at (a) $D_0 = 5{\cdot}2$ km/s and (b) $D_0 = 4{\cdot}0$ km/s.

interaction between the two materials is not seen, and why the measured shock angle is so sensitive to lot.

Acknowledgements

This work was performed at the Los Alamos National Laboratory, which is operated by the University of California for the US Department of Energy, under contract W-7405-ENG-36. We acknowledge the support of the Los Alamos ASC program.

References

1. L.L. Davis and L.G. Hill, ANFO cylinder tests. In: M.D. Furnish, N.N. Thadhani and Y. Horie (eds.), *Shock Compression of Condensed Matter*. American Institue of Physics (2002) pp. 165–168.
2. T.D. Aslam and J.B. Bdzil, Numerical and theoretical investigations on detonation-inert confinement interactions. In: *12th Symp. (Int.) on Detonation*. Arlington: Office of Naval Research (2002) in print.
3. P.P. Rao Streamline curvature and velocity gradient behind strong shocks. *AIAA J.* 11 (1973) 1352–1354.
4. J.B. Bdzil, Steady-state two-dimensional detonation. *J. Fluid Mech.* 108 (1981) 195–266.
5. J.B. Bdzil and T.D. Aslam, Detonation front models: theories and methods. Los Alamos: Los Alamos National Laboratory Report LA-UR-02-942 (2002) 51pp.
6. R. Menikoff and B.J. Plohr, The Riemann problem for fluid flow of real materials *Rev. Mod. Phys.* 61 (1989) 75–130.
7. M. Van Dyke, *Perturbation Methods in Fluid Mechanics*. California: Parabolic Press (1975) 271 pp.
8. G. Eden and R.A. Belcher, The effects of inert walls on the velocity of detonation in EDC35, an insensitive high explosive. In: *9th Symp. (Int.) on Detonation*. Arlignton: Office of Naval Research (1989) pp. 831–841.
9. A.M. Amd-El-Fattah, L.F. Henderson and A. Lozzi, Precursor shock waves at a slow–fast gas interface. *J. Fluid Mech.* 108 (1976) 157–176.
10. J.D. Cole and L.P. Cook, *Transonic Aerodynamics*. Amsterdam: Elsevier (1986) 473 pp.
11. E.M. Murman and J.D. Cole, Calculation of plane steady transonic flows. *AIAA J.* 9 (1971) 114–121.
12. R.A. Catanach and L.G. Hill, Diameter effect curve and detonation curvature measurements for ANFO. In: M.D. Furnish, N.N. Thadhani and Y. Horie (eds.), *Shock Compression of Condensed Matter*. American institute of Physics (2001) pp. 906–909.
13. J.B. Bdzil, T.D. Aslam, R.A. Catanach, L.G. Hill and M. Short, DSD front models: non-ideal explosive detonation in ANFO. Los Alamos: Los Alamos National Laboratory Report LA-UR-02-4332 (2002) 11 pp.